Fabrication of highly ordered Cu2+/Fe3+ decorated polyhedral oligomeric silsesquioxane hybrids

Potsi, Georgia; Wu, Jiquan; Portale, Giuseppe; Gengler, Regis Y. N.; Longo, Alessandro; Gournis, Dimitrios; Rudolf, Petra

Published in:
Journal of Colloid and Interface Science

DOI:
10.1016/j.jcis.2020.03.033

Publication date:
2020

Journal of Colloid and Interface Science 572 (2020) 207–215

Contents lists available at ScienceDirect

Journal of Colloid and Interface Science

journal homepage: www.elsevier.com/locate/jcis

Fabrication of highly ordered Cu^{2+}/Fe^{3+} decorated polyhedral oligomeric silsesquioxane hybrids: How metal coordination influences structure

Georgia Potsi [a,b,1], Jiquan Wu [a,1], Giuseppe Portale [a], Regis Y.N. Gengler [a], Alessandro Longo [c,d], Dimitrios Gournis [b,*], Petra Rudolf [a,*]

[a] Zernike Institute for Advanced Materials, University of Groningen, Nijenborgh 4, 9747 AG Groningen, the Netherlands
[b] Department of Materials Science & Engineering, University of Ioannina, GR-45110 Ioannina, Greece
[c] Department of Materials, Textiles and Chemical Engineering Technologiepark 125, 9052 University of Ghent, Belgium
[d] Istituto per lo Studio dei Materiali Nanostrutturati (ISMN)-CNR, UOS Palermo, Via Ugo La Malfa, 153, 90146 Palermo, Italy

GRAPHICAL ABSTRACT

Tuning the geometry of Langmuir Schaefer films by using polyhedral oligomeric silsesquioxanes decorated with different metal ions.

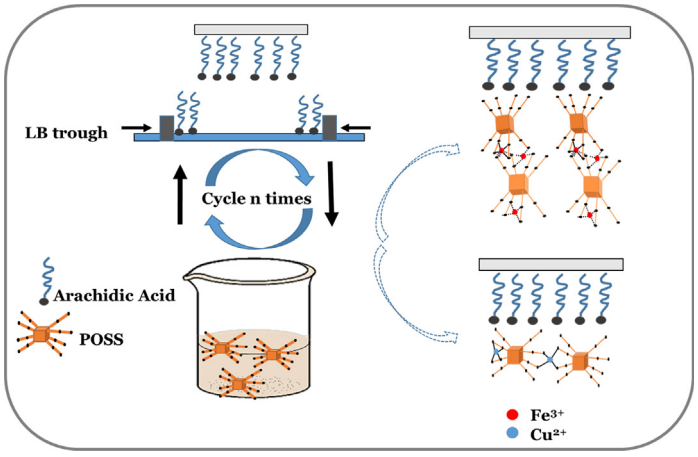

ARTICLE INFO

Article history:
Received 3 November 2019
Revised 17 February 2020
Accepted 8 March 2020
Available online 16 March 2020

ABSTRACT

Incorporation of isolated metal centers into well-organized nanostructures is a promising route in the development of the next generation of chemical, magnetic and electronic devices. In this work, a layer-by-layer protocol to grow highly ordered thin films of metal-decorated organic-inorganic cage-like polyhedral oligomeric silsesquioxane (POSS) is introduced. The key strategy is to use metal ions (Cu^{2+} or Fe^{3+}) as linker for the amino-functionalized cage-like POSS, which are self-assembled between arachidic acid layers during Langmuir–Schaefer deposition. The Langmuir–Schaefer films are examined

Abbreviations: POSS, polyhedral oligomeric silsesquioxane; AA, arachidic acid; LS, Langmuir-Schaefer; LB, Langmuir-Blodgett; SAM, self-assembly; XPS, X-ray photoelectron spectroscopy; XRD, X-ray diffraction; GIWAXS, Grazing incidence Wide-angle X-ray scattering; EXAFS, Extended X-Ray Absorption Fine Structure; XANES, X-ray Absorption Near Edge Spectroscopy.

* Corresponding authors.
E-mail addresses: dgourni@cc.uoi.gr (D. Gournis), p.rudolf@rug.nl (P. Rudolf).

[1] Georgia Potsi and Jiquan Wu have contributed equally to this work.

https://doi.org/10.1016/j.jcis.2020.03.033
0021-9797/

Keywords:
Langmuir Schaefer films
Silsesquioxanes
Metal complexes

by X-ray photoelectron spectroscopy, X-ray diffraction, grazing incidence wide-angle X-ray scattering and extended X-ray absorption fine structure in order to understand how the coordination of metal ions influences the structure in the course of the layer-by-layer formation of the films.

1. Introduction

Incorporating molecular building blocks with appropriate physical and chemical properties into a suitably prearranged host system in order to construct well-ordered thin films continues to be a major challenge in materials science and technology. This is especially true in the fields of electronics, catalysis and nanocomposites, where the structure of the resulting material is of crucial importance [1–4]. Particularly interesting building blocks in this context are polyhedral oligosilsesquioxanes (POSS), which derive from hydrolytic condensation reactions of organosilicon monomers ($RSiOH_3$) [4], and form three-dimensional (3D) cage-like highly symmetric frameworks, where an organic group is covalently attached to the Si-O-Si chain. Over the past two decades, POSS provided a versatile platform for innovative research with applications as diverse as aerospace [5], dentistry [6,7], protective coatings [4], microelectronics [8], catalysis [3,9,10], energy storage [11,12], environmental remediation [13,14], drug delivery [15,16] and biomedicine [14,17].

Moreover, POSS can bind metal ions forming metal decorated silsesquioxanes [3,13,18–20] that can serve as components of hybrid materials suitable for catalytic applications such as natural gas separation [21] or hydrogen catalysis [22]. In particular, amino-functionalized POSS structures constitute high affinity binding sites for metals, where the metal ions are bound in a single ligand (monodentate) via the amino group, thus resulting in maximum metal binding efficiency [3,23].

POSS hybrids are usually synthesized by conventional chemical copolymerization, crosslinking, or physical blending [1]; alternatively they can be used as cores for dendrimer synthesis [2]. Much research focuses on the bulk synthesis of polymer nanocomposites [23–26] and hybrid materials [23,27]. In contrast, there are few reports using a thin film approach, such as the Langmuir-Blodgett (LB) [28–33] or Langmuir Schaefer (LS) [30] methods. POSS derivatives have been found to self-assemble as monolayers at the air/water interface [34,35]. In fact, when hydrophilic hydroxyl groups are attached to the POSS cage, they can rest on the subphase, while organic R groups are hydrophobic and orient them away from the water surface. These amphiphilic properties of POSS allow the formation of Langmuir films [30,36].

Synthetic methods such as Langmuir Blodgett (LB) and Langmuir Schaefer (LS) deposition permit to form complex structures of desired thickness and architecture [37,38]. These methods also overcome a major problem in the preparation of POSS hybrids, which is the tendency of POSS to segregate and form aggregates causing inhomogeneity during film formation [32]. Controlling the structure through LB or LS deposition provides homogeneity as well as better reproducibility of the hybrid systems and hence warrants a better management of material properties [31,34].

Here we report on the assembly of metal-decorated (Cu^{2+} or Fe^{3+}) POSS between amphiphilic arachidic acid (AA) layers in order to form highly ordered hybrid films. We have achieved this by combining Langmuir-Schaefer (LS) deposition with self-assembly from solution.

Our aim was to investigate the final structure of hybrid thin films as well as to prove that by using metal ions with different coordination [39–41], the architecture of the thin films can be tailored. In particular, our hypothesis was that when using copper or iron complexes in the synthesis of metal decorated silsesquioxanes, the metal coordination of the two complexes determines the final structure of the films since it controls the bonds that can be formed between the metal complex and the amino groups of POSS. In the case of Cu-decorated POSS films, the trans square planar arrangement of $CuCl_2$ is governed by weak intermolecular Cu-Cl interactions and only four ligands can be replaced during the formation of copper-nitrogen bonds between copper-containing moieties and the amino species of POSS [2,42]. This should result in copper bound with four amine ligands of one POSS moiety or 4 amine ligands belonging to two POSS moieties oriented in parallel. On the other hand, iron complexes usually exist in octahedral coordination, or, in rare cases, in tetrahedral coordination [43]. Since six nitrogen ligands are present during the formation of Fe complexes [39–41], iron should bind to the nitrogen ligands of two POSS moieties. Altering the concentration of metal ions could lead to other results since the overall number of ligands of POSS that could participate in bonding would be different and hence affect the films structure especially in the case of iron but such a scenario was not examined in the current study. In order to prove our hypothesis, the metal decorated films were studied with different characterization techniques, including X-ray Photoelectron Spectroscopy (XPS), X-ray Diffraction (XRD) measurements, Grazing incidence Wide-angle X-ray scattering (GIWAXS) and Extended X-Ray Absorption Fine Structure (EXAFS). The importance of introducing this method lies on the potential use of these films in applications where layers of different nature and properties are required, such as in optics where the refractive index of the layers governs their reflective properties [44] or in sensors where the sensitivity changes of thin films are exploited for interaction with a gas environment [45].

2. Materials and preparation of films

Silicon wafers (Prime Wafer) served as substrates for the AA-Metal POSS hybrid films. The surface of substrates was made hydrophobic by self-assembly of octadecyltrichlorosilane (Sigma Aldrich, purity 99%) prior to LS film deposition. LS films were prepared on a Nima Technology thermostated 612D LB trough at a temperature of 23 ± 0.5 °C. Ultra-pure water with resistivity >18 MΩ cm was used to prepare the subphase. Arachidic acid (AA) (Merck, purity ≥ 99%) was dissolved in chloroform (Merck, purity ≥ 99%) to prepare a spreading solution of 0.2 mg/mL, 150 μL of which was deposited at the surface of the subphase with the help of a microsyringe. After a waiting time of 15 min, to allow for the solvent evaporation, the AA layer was compressed at a rate of 25 cm min^{-1} until the chosen stabilization pressure of 25 mN m^{-1} was reached. This pressure was maintained throughout the deposition process. Films were transferred onto the hydrophobic substrate by horizontal dipping, with downward and lifting speeds of 4 mm min^{-1} and 2 mm min^{-1}, respectively. Each time the substrate was lowered into the LB trough, it was allowed to touch the air-water interface in a very gentle dip of max 0.5 mm below the water level and then rinsed several times by dipping into ultrapure water. Synthesis of metal

POSS complexes was performed by controlled hydrolysis of 3-(2-aminoethylamino)-propyltrimethoxysilane (Sigma-Aldrich, purity 98%) in an ethanol (Sigma-Aldrich, ≥ 99%)/d.d.water (14:1 v/v) solvent mixture to give a solution of concentration 0.45 M. Next 30 mL of an aqueous 0.1 M $FeCl_2$ (Merck, purity ≥ 99%) or 0.1 M $CuCl_2$ (Acros, purity ≥ 99%) solution was reacted with 20 mL and 13.5 mL of the above solution respectively upon stirring. The produced metal-POSS complexes were used 24 h after their formation. The final surface was again rinsed copiously with pure water and dried by blowing with N_2. To deposit multilayer films, one simply repeats the whole cycle as many times as needed (see Scheme 1).

3. Experimental techniques

X-Ray Photoelectron Spectroscopy (XPS) data were collected using a Surface Science SSX-100 ESCA instruments with a monochromatic Al Kα X-ray source (hν = 1486.6 eV) operating at a base pressure of $\approx 5 \times 10^{-10}$ mbar. The energy resolution was set to 1.26 eV and the electron take-off angle was 37° with respect

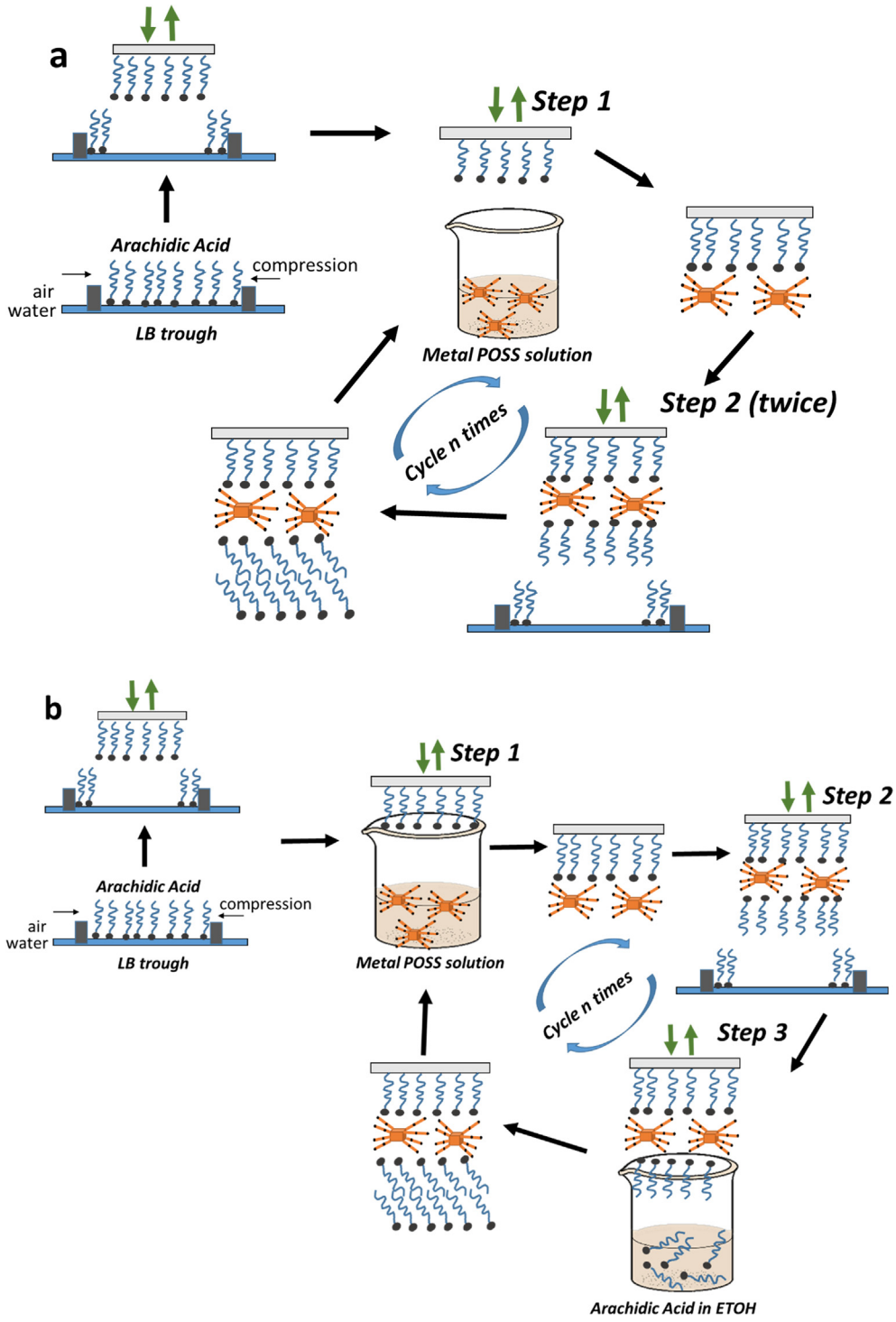

Scheme 1. (Color online) Fabrication of LS AA-metal (Cu^{2+} or Fe^{3+})-POSS films by **Synthetic route 1** (a) and **Synthetic route 2** (b).

to the surface normal. The XPS spectra were analyzed using the least-squares curve fitting program Winspec, developed at the LISE laboratory, University of Namur, Belgium. Binding energies deduced from curve fitting are reported to a precision of ±0.1 eV and referenced to the C1*s* photoemission peak at 284.5 eV [46]. All measurements were carried out on freshly prepared samples, 3 different spots were measured on each sample to check for homogeneity.

X-ray Diffraction (XRD) experiments were carried out on 20 layer-thick AA-Metal POSS hybrid films. The out of plane XRD data for the hybrid films were collected under ambient conditions with a Philips PANanalytical X'Pert MRD diffractometer. A Cu Kα (λ = 1.5418 Å) radiation source was used (operated at 40 kV, 40 mA); a 0.25° divergence slit and a 0.125° anti scattering slit were employed. The 2θ scans were performed from 0.6° to 15° with a 0.02° step and a counting time of 15 s per step.

Grazing-incidence Wide-angle X-ray scattering (GIWAXS) experiments were performed at the Dutch-Belgian beamline BM26B (DUBBLE) at the European Synchrotron Radiation Facility (ESRF). The X-ray photon wavelength used was λ = 0.1 nm. The GIWAXS patterns were acquired using a Frelon2K CCD detector placed 85 mm away from the sample. The beam center and the sample-to-detector distance were determined using the diffraction rings from a standard silver behenate powder sample. The multilayered samples were placed under an incident angle α_i = 0.15° with respect to the incoming beam using a motorized Huber semicircular goniometer. The GIWAXS images are presented as a function of the quasi-vertical and horizontal scattering vector q_z and q_y, related to the exit angles in the vertical and horizontal direction α_f and $2\theta_f$, respectively:

$$q_y = \frac{2\pi}{\lambda}(\cos(\alpha_f)\sin(2\theta_f))$$

$$q_z = \frac{2\pi}{\lambda}(\sin(\alpha_f) + \sin(\alpha_i))$$

The GIWAXS images were corrected for the detector dark current, flat field and air background scattering, before plotting them and performing the intensity cuts. The vertical intensity cuts presented here were calculated at q_y = 0 nm^{-1} by averaging the intensity of 4 adjacent columns of pixels.

X-ray Absorption Near Edge Spectroscopy (XANES) and Extended X-ray Absorption Fine Structure (EXAFS) spectra were collected at BM26A, the Dutch-Belgian beamline (DUBBLE) at the European Synchrotron Radiation Facility (ESRF) at the Fe K-edge (7112 eV) and at the Cu K-edge (8979 eV), respectively. The energy of the X-ray beam was tuned by a double-crystal monochromator operating in fixed-exit mode using a Si(1 1 1) crystal pair. XANES spectra were analysed based on XPS deconvolution and dominant species of Fe^{3+} and Cu^{2+}.The EXAFS spectra of the multilayered samples were collected in fluorescence mode using a 9-element Ge detector (Ortec Inc.). Reference spectra of the two metal foils, copper and iron, (Sigma Aldrich) were measured in transmission mode using Ar/He-filled ionization chambers at RT.

4. Results and discussion

Prior to the fabrication of the thin films examined in this study, deposition experiments were performed to determine the ordering and the potential structure of the metal-POSS films. In order to achieve the best ordering, we followed two fabrication protocols using the LS technique. One protocol introduced a self-assembly step during the layer deposition and the other without such a step. We compared the XRD results of the fabricated films. In both cases, the substrate was first rendered hydrophobic as explained in the section Methods of preparation/Experimental techniques. In **Synthetic route 1** (Scheme 1**a**), after a Langmuir film was transferred to the substrate, a layer of metal-decorated (Cu^{2+} or Fe^{3+})-POSS was formed on the AA-covered substrate by self-assembly during immersion (immersion time 2 min) in a solution of the metal-decorated silsesquioxane (step 1), then two AA monolayers were added by LS deposition (step 2, repeated twice). The synthesis continued by repeating steps 1 and 2 to build up a thicker film. In **Synthetic route 2 (**Scheme 1**b**), after transferring the AA Langmuir film to the substrate and depositing the (Cu^{2+} or Fe^{3+})-POSS by self-assembly (step 1, immersion time 2 min) one AA monolayer is deposited by LS deposition (step 2), and a third step was added (step 3) consisting in the self-assembly of an extra layer of AA by contacting the substrate with a AA bearing solution (immersion time 2 min, AA in ethanol, concentration of 0.5 mg/mL). The film was built up by repeating the sequence step 1 – step 2 – step 3. Further details of the deposition, such as the transfer ratio at each step and the surface pressure during the deposition, are reported in the Supporting Information (**Fig. S1**).

From XRD results (Fig. 1) it is obvious that the fabrication route that includes the AA self-assembly step leads to more ordered films since their d_{001} diffraction peak is sharper than that of films where the fabrication procedure comprised no self assembly step (Fig. 1). This means that the AA molecules are better organized when the second layer of the surfactant is formed by contacting the surface of the AA bearing solution (Scheme 1**b, Synthetic route** 2, step 3). We therefore adopted **Synthetic route 2 (**Scheme 1**b**) as deposition protocol for our study.

When comparing the Cu- and Fe-containing films, we found that those synthesized using copper decorated silsesquioxanes exhibit the d_{001} diffraction peak at 2.37 ± 0.02°, which translates to a 37.9 ± 0.3 Å spacing. For those synthesized using iron decorated silsesquioxanes, the diffraction peak appears at much lower angles (1.37 ± 0.02°), implying a spacing of about 64.5 ± 0.9 Å (Fig. 1). The length of AA monolayers can vary from 25 to 15 Å depending on the tilt angle of the molecules in the film [47]. Different orientation of AA molecules during the deposition process could cause differences in spacing between layers. Though, the fact that the concentration of AA was kept the same for both synthetic routes, suggests that the AA bilayer is tilted in the same way in both cases and that the 27 Å difference in spacing derives from a different conformation of the metal decorated silsesquioxane layer for different metals. In fact, Balomenou et al. [23] found that the interlayer space of clays intercalated with silsesquioxanes increased by 7.1 Å, which corresponds to the silsesquioxanes size when their flexible side chains take a horizontal orientation. Instead, Kataoka et al. [48], who also prepared layered organic-inorganic hybrid materials with functionalized silsesquioxanes as intercalant, showed that the space occupied when the side chains take a vertical orientation, is 17–17.6 Å (Scheme 2). Accepting these values as representing the dimensions of POSS, the XRD results lead us to assume that when Cu-POSS is used, the copper binds either with four amine ligands of one POSS or 4 amine ligands belonging to two parallel POSS moieties. In the case of iron, where metal coordination is octahedral, six ligands can be replaced during the formation of the metal decorated silsesquioxane and iron binds with the amine groups of two POSS moieties (Scheme 2). Moreover, the increased spacing suggests that Fe-POSS moieties position themselves in a stacked fashion during the deposition process as sketched in the inset of Fig. 1, thereby increasing the interlayer spacing of the film**.**

In order to verify the successful insertion of metal POSS moieties in our films, X-ray Photoelectron Spectroscopy (XPS) was employed. Fig. 2**a,b** shows the XPS surveys spectra of fabricated films following **Synthetic route 2.** The wide scan spectra show the fingerprint of all the elements expected in AA-Metal-POSS hybrid films: C, N, Si, Cu/Fe (annotated). Moreover, the high resolu-

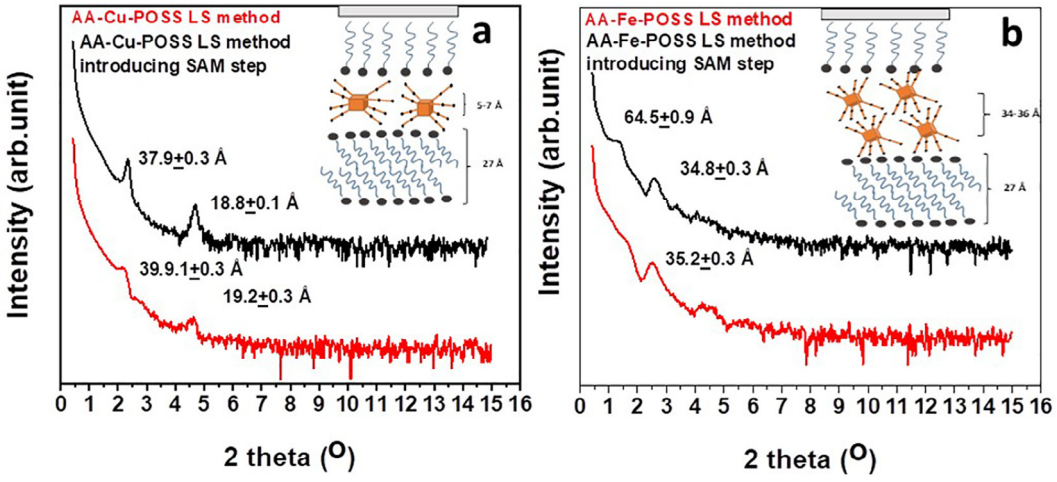

Fig. 1. (Color online) XRD patterns of multilayers of (a) AA-Cu-POSS and (b) AA-Fe-POSS deposited following **Synthetic routes 1** (red) and **Synthetic route 2** (black); insets: possible structure of LS films.

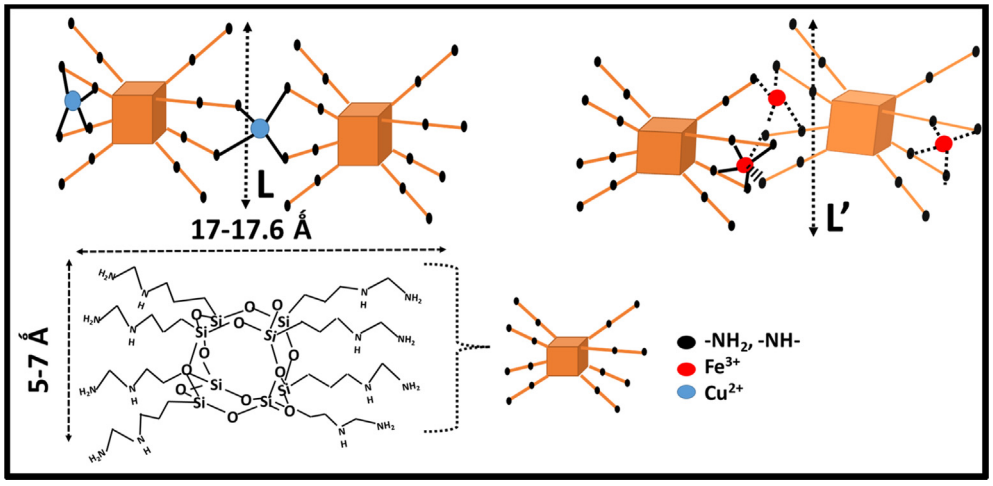

Scheme 2. (Color online) Top: Potential structures and metal bonding of the metal (Cu^{2+}, Fe^{3+}) decorated POSS depending on the metal coordination (planar for Cu, tetrahedral or octahedral for Fe); Bottom: dimensions of POSS.

tion spectra of the Fe2*p* and Cu2*p* (Fig. 2c,d) as well as the N1*s* (Fig. 2e,f) core level regions confirm the presence and thus the successful attachment of metal decorated POSS onto the AA molecules during the formation of the thin films. In detail, in Fig. 2c the deconvolution of Fe2*p* core level region shows two chemical states for iron (Fe^{3+} and Fe^{2+}) with Fe^{3+} being the dominant species (82.2%). Similarly, in Fig. 2d, deconvolution of Cu2*p* reveals the existence of $Cu^{2+}$and Cu^{+} metal ions in a rate of 73.6% and 26.4%, respectively. Additionally, N1s high resolution spectra (Fig. 2e,f) reveal the formation of Metal-POSS bonds through NH/NH_2 –and Cu^{2+} or Fe^{3+} metal ions interactions [49] and the presence of a small amount of protonated amines.

In order to elucidate the structural order of the hybrid films, 5 and 25 layer- thick films of AA-Cu-POSS and AA-Fe-POSS were further analyzed by Grazing-Incidence Wide-Angle X-ray Scattering (GIWAXS). The results are shown in Fig. 3. GIWAXS is a powerful tool to investigate layered systems, such as supported smectic-A crystalline polymer systems [50,51]. The GIWAXS patterns of AA-Cu-POSS and AA-Fe-POSS films demonstrate the good orientational order of these multilayered structures. As expected, the diffraction signals of the interlayer spacing are strongly focused along the vertical q_z direction, indicating the layers align in a parallel fashion with respect to the substrate. Generally, the 5-layer samples show better ordering as evident for the AA-Cu-POSS 5 layer sample, where sharp spots indicative for the (partial) crystallization of the AA aliphatic chains are observed. The Cu-containing films show better order than the ones comprising Fe. While the 25-layer AA-Cu-POSS film shows still good ordering, the 25-layer-AA-Fe-POSS film exhibits an isotropic structure, which can suggest that the way Fe is coordinated differs from that of Cu and indicates that both the AA and POSS take different orientations during the formation of multilayers (see XANES results below).

The corresponding vertical intensity cuts along q_z for the AA-Cu-POSS and AA-Fe-POSS samples as shown in Fig. 4. In the left panel, which refers to AA-Cu-POSS films, the first order diffraction peak of the 5 layer-thick film is found at 1.81 ± 0.5 nm^{-1} and that for the 25 layer-thick film at 1.67 ± 0.5 nm^{-1}, corresponding to a repeat unit spacing of 3.45 ± 0.5 nm (34.5 ± 5 Å) and 3.76 ± 0.5 n m (37.6 ± 5 Å), respectively. The results are in good agreement with the XRD results (~3.77 nm for a 20-layer film of AA-Cu-POSS). The right panel of Fig. 4 presents the results for AA-Fe-POSS films. Here, the first order diffraction peaks are not in the probed range, but the

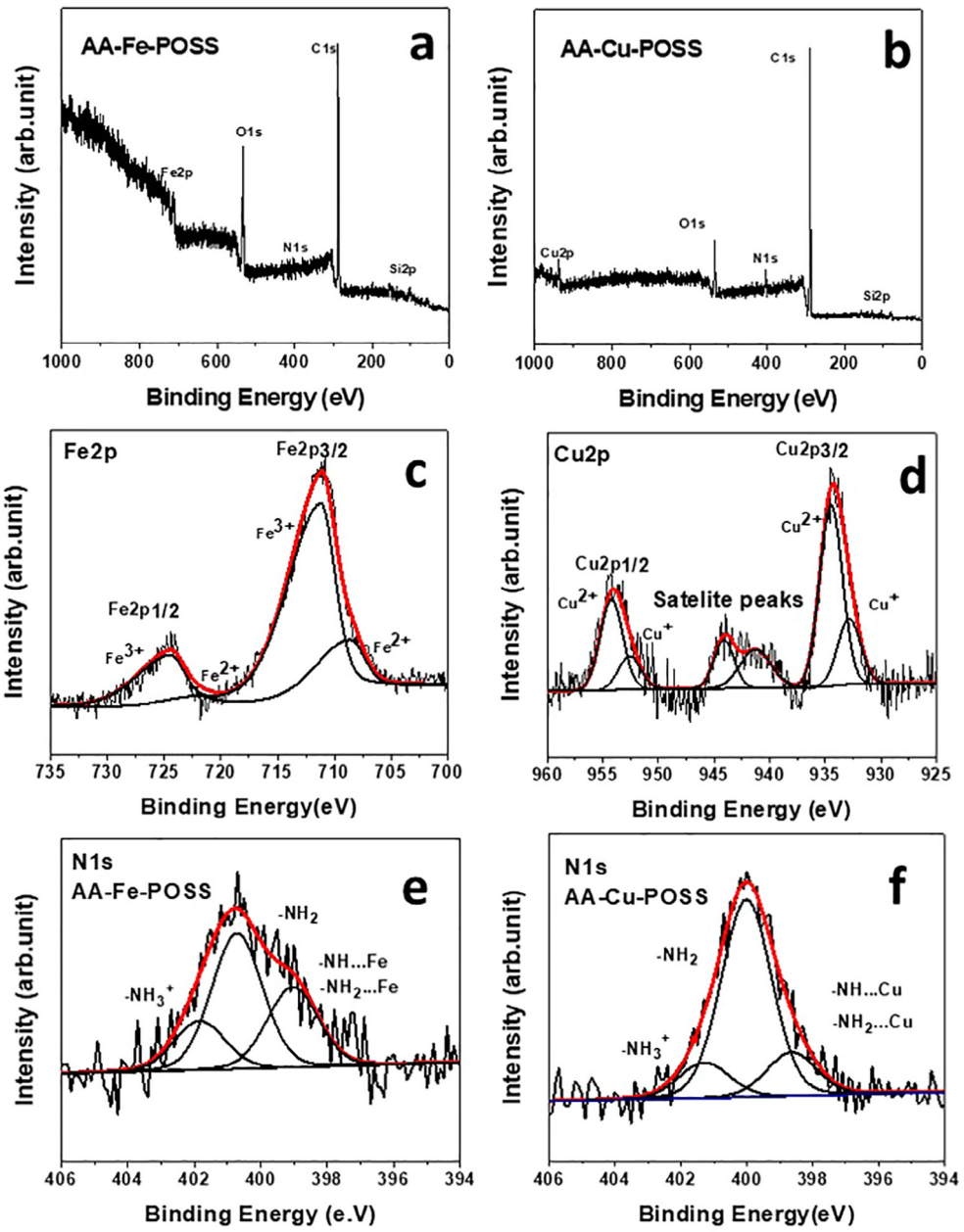

Fig. 2. (Color online) Wide scan XPS spectra of (a) AA-Fe-POSS and (b) AA-Cu-POSS multilayers deposited following **Synthetic route 2**; detailed XPS spectra of the (c) Fe2*p* and (d) Cu2*p* core level region for the same AA-Fe-POSS and AA-Cu-POSS films**,** detailed XPS spectra of the N1*s* core level region for AA-Fe-POSS (e) and AA-Cu-POSS (f) films.

second order diffraction peaks at 1.65 nm^{-1} and 1.85 nm^{-1} are visible (marked with stars). The corresponding spacings are 7.60 ± 0. 5 nm (76.5 ± 5 Å) and 6.78 ± 0.5 nm (67.8 ± 5 Å) for the 5 and 25 layers, respectively. Also in this case there is good agreement with the XRD results (~6.80 nm for 20-layer of AA-Fe-POSS). Interestingly, the broadening of the interlayer peaks and the orientational disorder for the AA-Fe-POSS samples is always higher than for the Cu samples.

In order to study the coordination geometry of the metal centers decorating POSS, we conducted an X-ray absorption near edge structure (XANES) investigation. Fig. 5 shows the XANES spectra for the AA-metal-POSS multilayered structures with 25 layers. To elucidate the local environment and the implications of the insertion of the metals for the electronic structure, XANES simulations were performed using the FDMNES program using the multiple scattering theory based on the muffin-tin approximation for the potential shape [52].

The muffin-tin radii were tuned to have a 10% overlap between the different spherical potentials. Octahedral, planar and tetrahedral coordination geometries for both Cu and Fe cations were simulated, using a metal-N bond distance of 2.0 Å for all the three structures. In Fig. 5, we report the simulations that best agree with the experimental XANES data. The XANES simulations suggest that the larger layer spacing and the lower degree of orientational order of the multilayered AA-Fe-POSS structure are related to a difference in the metal coordination. Simulations point to a prevalently planar geometry of the Cu metal centers, most probably coordinating only two amine ligands of one POSS moiety or two amine ligands of two adjacent POSS moieties contained within the same layer. Particularly indicative of the planar configuration, is the

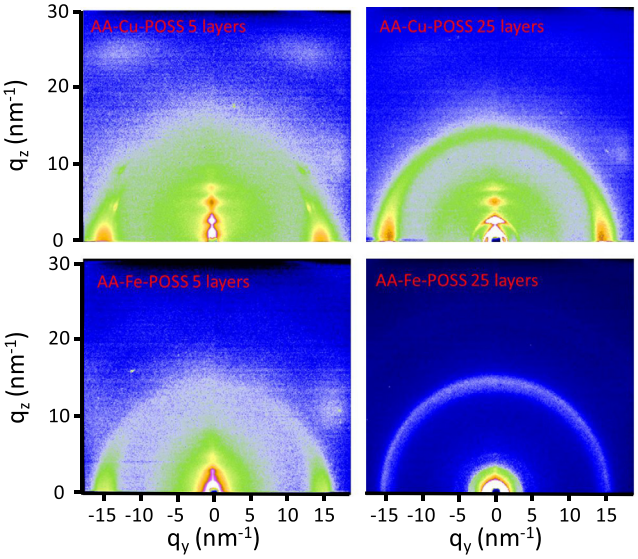

Fig. 3. (Color online) The 2D GIWAXS patterns of AA-Cu-POSS (5 and 25 layers) and AA-Fe-POSS (5 and 25 layers) samples.

shoulder located at about 8988 eV. This Cu-POSS coordination geometry leads to an ordered structure with parallel layers, where the Cu-POSS complexes are sandwiched between the organic layers. On the contrary, simulations show a more complex situation for the AA-Fe-POSS films. The main features of the Fe XANES spectrum agree well with an octahedral geometry, while the relative intensities of the various spectral features are more in agreement with a tetrahedral geometry. Thus, the AA-Fe-POSS film most probably contains iron atoms in both octahedral and tetrahedral geometry. In both cases, the iron geometry is far from planar and the iron metal centers coordinate more than two POSS molecules with different orientation with respect to the organic layers, thus hindering the formation of an ordered structure with parallel layers.

5. Conclusions

We successfully fabricated multilayer films of well-ordered metal-decorated (Cu^{2+} and Fe^{+3}) polyhedral oligomeric silsesquioxanes (POSS) and arachidic acid by using two modified Langmuir-Schaefer deposition protocols. The main goal was to build up homogeneous well-ordered films by exploiting metal ions coordination properties. Both protocols start with LS deposition of arachidic acid followed by self-assembly of a metal-decorated (Cu^{2+} or Fe^{3+})-POSS monolayer but differ in the arrangement of the next arachidic acid layer on top of the POSS surface. XPS study confirmed the successful coordination of metals with the POSS as well as the successful attachment of metal-POSS to AA molecules. Using XRD, we showed that hybrid films deposited following the synthetic route involving Langmuir Schaefer deposition alternated with self-assembly steps lead to better ordered structures. In addition, XRD results suggested that the interlayer distance between the layers differs because of the different metal coordination of the Cu^{2+} and Fe^{3+} ions. GIWAXS and XANES measurements allowed for further insight into the multilayer ordering and the metal coordination in our hybrid AA-metal-POSS films corroborating the XPS results. A four-fold planar coordination for the Cu-POSS and a combination of tetrahedral and octahedral coordination for the Fe-POSS were observed. This change in coordination is responsible for the large difference in layer spacing and orientational order of the Cu- and the Fe-containing hybrid multilayers. Overall, we show that by employing LS deposition combined with self-assembly and exploiting metal ion coordination properties, we are able to produce homogenous and reproducible hybrid systems with desirable and tuned architecture. Further research could determine not only the effect of coordination number of Fe and Cu ions on the geometry of the films but also the effect that different concentration of ions could cause regarding the orientation of the forming layers. This key property is highly important in a number of applications where thin films are used (*e.g.* electronics) and pave the way for the development of a new class of hybrid systems where highly ordered incorporation of building blocks such as POSS is crucial

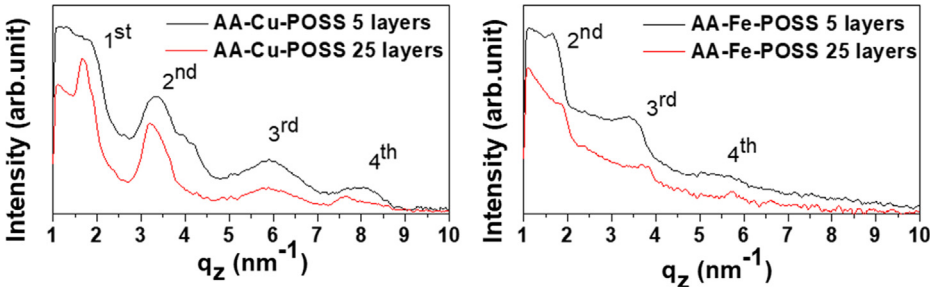

Fig. 4. (Color online) GIWAXS vertical intensity cuts (q_z scans) of 5 and 25 layers AA-Cu-POSS films (left panel) and 5 and 25 layers AA-Fe-POSS films (right panel).

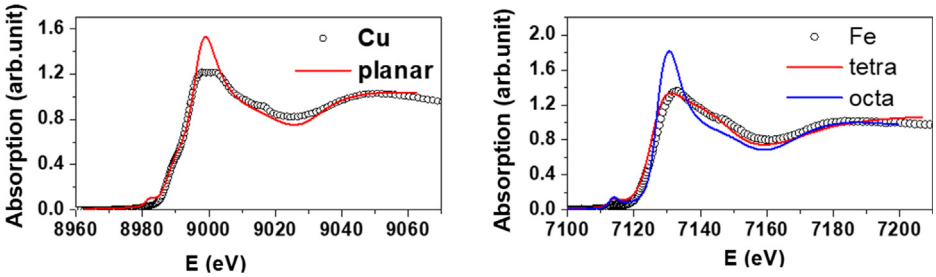

Fig. 5. (Color online) XANES absorption spectra for 25 layer-thick AA-Cu-POSS and the AA-Fe-POSS films plotted together with the simulated XANES spectra for the metal geometries that best approximate the experimental data.

[53,54]. Moreover, tuning the film geometry using different metal ions can be a potential synthesis alternative for applications where a diverse refractive index and layer thickness are required.

6. Credit author statement

Georgia Potsi and Jiquan Wu fabricated the L.S films and performed XPS and XRD measurements, Giuseppe Portale and Alessandro Longo performed the GIWAXS, EXAFS and XANES measurements, Regis Y.N. Gengler contributed in the design and methodology of the project, Petra Rudolf and Dimitrios Gournis designed and supervised the project. All authors contributed in writing, reviewing and editing the manuscript.

Declaration of Competing Interest

The authors declare that there is no conflict of interest.

Acknowledgements

The authors thank Prof. Beatriz Noheda and Mart Salverda for the assistance provided during XRD experiments. G.P. acknowledges support from the Ubbo Emmius Fund of the University of Groningen. J.Wu acknowledges the China Scholarship Council (CSC) for supporting his PhD study. This work was performed within the "Top Research School" programme of the Zernike Institute for Advanced Materials under the Bonus Incentive Scheme (BIS) of the Netherlands' Ministry of Education, Science, and Culture.

Appendix A. Supplementary material

Supplementary data to this article can be found online at https://doi.org/10.1016/j.jcis.2020.03.033.

References

[1] W. Zhang, A.H.E. Müller, A "Click Chemistry" approach to linear and star-shaped telechelic POSS-containing hybrid polymers, Macromolecules 43 (2010) 3148–3152, https://doi.org/10.1021/ma902830f.
[2] K. Naka, M. Fujita, K. Tanaka, Y. Chujo, Water-soluble anionic POSS-core dendrimer: synthesis and Copper(II) complexes in aqueous solution, Langmuir 23 (2007) 9057–9063, https://doi.org/10.1021/la7013286.
[3] G. Potsi, A.K. Ladavos, D. Petrakis, A.P. Douvalis, Y. Sanakis, M.S. Katsiotis, G. Papavassiliou, S. Alhassan, D. Gournis, P. Rudolf, Iron-substituted cubic silsesquioxane pillared clays: synthesis, characterization and acid catalytic activity, J. Colloid Interface Sci. 510 (2018) 395–406, https://doi.org/10.1016/j.jcis.2017.09.003.
[4] R.H. Baney, M. Itoh, A. Sakakibara, T. Suzuki, Silsesquioxanes, Chem. Rev. 95 (1995) 1409–1430, https://doi.org/10.1021/cr00037a012.
[5] S.H. Phillips, T.S. Haddad, S.J. Tomczak, Developments in nanoscience: polyhedral oligomeric silsesquioxane (POSS)-polymers, Curr. Opin. Solid State Mater. Sci. 8 (2004) 21–29, https://doi.org/10.1016/j.cossms.2004.03.002.
[6] M.S. Soh, A.S., A.U.J. Yap, Dental Nanocomposites, Curr. Nanosci. 2 (2006) 373–381. https://doi.org/http://dx.doi.org/10.2174/157341306778699365.
[7] H. Fong, S.H. Dickens, G.M. Flaim, Evaluation of dental restorative composites containing polyhedral oligomeric silsesquioxane methacrylate, Dent. Mater. 21 (2005) 520–529, https://doi.org/10.1016/j.dental.2004.08.003.
[8] Y.-T. Chang, C.-F. Shu, C.-M. Leu, K.-H. Wei, Synthesis and characterization of hyperbranched aromatic poly(ether imide)s with terminal amino groups, J. Polym. Sci. Part A Polym. Chem. 41 (2003) 3726–3735, https://doi.org/10.1002/pola.10939.
[9] F. Carniato, C. Bisio, G. Gatti, E. Boccaleri, L. Bertinetti, S. Coluccia, O. Monticelli, L. Marchese, Titanosilsesquioxanes embedded in synthetic clay as a hybrid material for polymer science, Angew. Chem. 121 (2009) 6175–6177, https://doi.org/10.1002/ange.200901927.
[10] N.N. Ghosh, J.C. Clark, G.T. Eldridge, C.E. Barnes, Building block syntheses of site-isolated vanadyl groups in silicate oxides, Chem. Commun. (2004) 856–857, https://doi.org/10.1039/B316184F.
[11] J. Zhang, X. Li, Y. Li, H. Wang, C. Ma, Y. Wang, S. Hu, W. Wei, Cross-linked nanohybrid polymer electrolytes with POSS cross-linker for solid-state lithium ion batteries, Front. Chem. 6 (2018) 186, https://doi.org/10.3389/fchem.2018.00186.
[12] H.-L. Chen, X.-N. Jiao, J.-T. Zhou, The research progress of polyhedral oligomeric silsesquioxane (POSS) applied to electrical energy storage elements, Funct. Mater. Lett. 10 (2017) 1730001, https://doi.org/10.1142/S1793604717300018.
[13] G. Potsi, A. Rossos, A. Kouloumpis, M.K. Antoniou, K. Spyrou, M.A. Karakassides, D. Gournis, P. Rudolf, Carbon nanostructures containing polyhedral oligomeric silsesquioxanes (POSS), Curr. Org. Chem. 20 (2016) 662–673, https://doi.org/10.2174/1385272819666151006010352.
[14] H. Ghanbari, B.G. Cousins, A.M. Seifalian, A nanocage for nanomedicine: polyhedral oligomeric silsesquioxane (POSS), Macromol. Rapid Commun. 32 (2011) 1032–1046, https://doi.org/10.1002/marc.201100126.
[15] Ł. John, M. Malik, M. Janeta, S. Szafert, First step towards a model system of the drug delivery network based on amide-POSS nanocarriers, RSC Adv. 7 (2017) 8394–8401, https://doi.org/10.1039/C6RA26330E.
[16] C. McCusker, J.B. Carroll, V.M. Rotello, Cationic polyhedral oligomeric silsesquioxane (POSS) units as carriers for drug delivery processes, Chem. Commun. (2005) 996–998, https://doi.org/10.1039/B416266H.
[17] M. Rojewska, M. Skrzypiec, K. Prochaska, The wetting properties of Langmuir-Blodgett and Langmuir-Schaefer films formed by DPPC and POSS compounds, Chem. Phys. Lipids. 221 (2019) 158–166, https://doi.org/10.1016/j.chemphyslip.2019.04.004.
[18] Y. Kaneko, E.B. Coughlin, T. Gunji, M. Itoh, K. Matsukawa, K. Naka, Silsesquioxanes: recent advancement and novel applications, Int. J. Polym. Sci. 2 (2012), https://doi.org/10.1155/2012/453821.
[19] D.B. Cordes, P.D. Lickiss, F. Rataboul, Recent developments in the chemistry of cubic polyhedral oligosilsesquioxanes, Chem. Rev. 110 (2010) 2081–2173, https://doi.org/10.1021/cr900201r.
[20] P.L. Almeida Júnior, C.H.S. Mendes, I.A.F.S. Lima, M.F. Belian, S.C.B. Oliveira, C. M.A. Brett, V.B. Nascimento, Ferricyanide confined in a protonated amine-functionalized silica film on gold: application to electrocatalytic sensing of nitrite ions, Anal. Lett. 51 (2018) 496–511, https://doi.org/10.1080/00032719.2017.1329834.
[21] F. Li, Y. Li, T.-S. Chung, S. Kawi, Facilitated transport by hybrid POSS®–Matrimid®–Zn2+ nanocomposite membranes for the separation of natural gas, J. Memb. Sci. 356 (2010) 14–21, https://doi.org/10.1016/j.memsci.2010.03.021.
[22] A. Maiti, R.H. Gee, R. Maxwell, A.P. Saab, Hydrogen catalysis and scavenging action of Pd-POSS nanoparticles, Chem. Phys. Lett. 440 (2007) 244–248, https://doi.org/10.1016/j.cplett.2007.04.045.
[23] G. Balomenou, P. Stathi, A. Enotiadis, D. Gournis, Y. Deligiannakis, Physicochemical study of amino-functionalized organosilicon cubes intercalated in montmorillonite clay: H-binding and metal uptake, J. Colloid Interface Sci. 325 (2008) 74–83, https://doi.org/10.1016/j.jcis.2008.04.072.
[24] K.J. Shea, D.A. Loy, Bridged polysilsesquioxanes. molecular-engineered hybrid organic−inorganic materials, Chem. Mater. 13 (10) (2001) 3306–3319, https://doi.org/10.1021/cm011074s.
[25] S.W. Kuo, F.C. Chang, POSS related polymer nanocomposites, Prog. Polym. Sci. 36 (2011) 1649–1696, https://doi.org/10.1016/j.progpolymsci.2011.05.002.
[26] G. Li, L. Wang, H. Ni, C.U. Pittman, Polyhedral Oligomeric Silsesquioxane (POSS) Polymers and Copolymers: A Review, J. Inorg. Organomet. Polym. 11 (n.d.) 123–154. https://doi.org/10.1023/A:1015287910502.
[27] Y. Xue, Y. Liu, F. Lu, J. Qu, H. Chen, L. Dai, Functionalization of graphene oxide with polyhedral oligomeric silsesquioxane (POSS) for multifunctional applications, J. Phys. Chem. Lett. 3 (2012) 1607–1612, https://doi.org/10.1021/jz3005877.
[28] W. Yin, J. Deng, A.R. Esker, Surface rheology of trisilanolisobutyl−POSS at the air/water interface, Langmuir 25 (2009) 7181–7184, https://doi.org/10.1021/la900397r.
[29] W. Lee, S. Ni, J. Deng, B.-S. Kim, S.K. Satija, P.T. Mather, A.R. Esker, Telechelic Poly(ethylene glycol)−POSS amphiphiles at the air/water interface, Macromolecules 40 (2007) 682–688, https://doi.org/10.1021/ma0618171.
[30] A. Wamke, K. Dopierała, K. Prochaska, H. Maciejewski, A. Biadasz, A. Dudkowiak, Characterization of Langmuir monolayer, Langmuir-Blodgett and Langmuir-Schaefer films formed by POSS compounds, Colloids Surf. A Physicochem. Eng. Asp. 464 (2015) 110–120, https://doi.org/10.1016/j.colsurfa.2014.10.022.
[31] A.C. Kucuk, J. Matsui, T. Miyashita, Langmuir-Blodgett films composed of amphiphilic double-decker shaped polyhedral oligomeric silsesquioxanes, J. Colloid Interface Sci. 355 (2011) 106–114, https://doi.org/10.1016/j.jcis.2010.12.033.
[32] M. Mitsuishi, F. Zhao, Y. Kim, A. Watanabe, T. Miyashita, Preparation of ultrathin silsesquioxane nanofilms via polymer Langmuir−Blodgett Films, Chem. Mater. 20 (2008) 4310–4316, https://doi.org/10.1021/cm800067j.
[33] M.K. Ferguson-McPherson, E.R. Low, A.R. Esker, J.R. Morris, Sorption of dimethyl methylphosphonate within Langmuir−Blodgett films of trisilanolphenyl polyhedral oligomeric silsesquioxane, J. Phys. Chem. B. 109 (2005) 18914–18920, https://doi.org/10.1021/jp0521959.

[34] J.R. Hottle, H.-J. Kim, J. Deng, C.E. Farmer-Creely, B.D. Viers, A.R. Esker, Blends of Amphiphilic PDMS and trisilanolisobutyl-POSS at the air/water interface, Macromolecules 37 (2004) 4900–4908, https://doi.org/10.1021/ma049511m.
[35] J. Deng, B.D. Viers, A.R. Esker, J.W. Anseth, G.G. Fuller, Phase behavior and viscoelastic properties of trisilanolcyclohexyl-POSS at the air/water interface, Langmuir 21 (2005) 2375–2385, https://doi.org/10.1021/la047568w.
[36] A.R. Esker, H. Yu, Langmuir Monolayers of Siloxanes and Silsesquioxanes BT - Silicone Surface Science, in: J.M. Owen, R.P. Dvornic (Eds.), Springer Netherlands, Dordrecht, 2012: pp. 195–228. https://doi.org/10.1007/978-94-007-3876-8_7.
[37] A. Kouloumpis, K. Spyrou, K. Dimos, V. Georgakilas, P. Rudolf, D. Gournis, A bottom-up approach for the synthesis of highly ordered fullerene-intercalated graphene hybrids, Front. Mater. 2 (2015) 10.
[38] A. Kouloumpis, N. Vourdas, P. Zygouri, N. Chalmpes, G. Potsi, V. Kostas, K. Spyrou, V.N. Stathopoulos, D. Gournis, P. Rudolf, Controlled deposition of fullerene derivatives within a graphene template by means of a modified Langmuir-Schaefer method, J. Colloid Interface Sci. 524 (2018) 388–398, https://doi.org/10.1016/j.jcis.2018.04.049.
[39] M. Balamurugan, P. Vadivelu, M. Palaniandavar, Iron(iii) complexes of tripodal tetradentate 4N ligands as functional models for catechol dioxygenases: the electronic vs. steric effect on extradiol cleavage, Dalt. Trans. 43 (2014) 14653–14668, https://doi.org/10.1039/C3DT52145A.
[40] D.M. Collins, R. Countryman, J.L. Hoard, Stereochemistry of low-spin iron porphyrins. I. Bis(imidazole).alpha.,beta.,gamma.,delta.-tetraphenylporphinatoiron(III) chloride, J. Am. Chem. Soc. 94 (1972) 2066–2072, https://doi.org/10.1021/ja00761a045.
[41] E.L. Rue, K.W. Bruland, Complexation of iron(III) by natural organic ligands in the Central North Pacific as determined by a new competitive ligand equilibration/adsorptive cathodic stripping voltammetric method, Mar. Chem. 50 (1995) 117–138, https://doi.org/10.1016/0304-4203(95)00031-L.
[42] C. Housecroft, Inorganic Chemistry, 3/E, third ed., Prentice Hall, Upper Saddle River, N.J., 2007.
[43] R.B. Bedford, P.B. Brenner, D. Elorriaga, J.N. Harvey, J. Nunn, The influence of the ligand chelate effect on iron-amine-catalysed Kumada cross-coupling, Dalt. Trans. 45 (2016) 15811–15817, https://doi.org/10.1039/C6DT01823H.
[44] J.-H. Kim, S. Fujita, S. Shiratori, Design of a thin film for optical applications, consisting of high and low refractive index multilayers, fabricated by a layer-by-layer self-assembly method, Colloids Surf. A Physicochem. Eng. Asp. 284–285 (2006) 290–294, https://doi.org/10.1016/j.colsurfa.2005.11.081.
[45] K. Schneider, M. Lubecka, A. Czapla, VOx thin films for gas sensor applications, Procedia Eng. 120 (2015) 1153–1157, https://doi.org/10.1016/j.proeng.2015.08.1009.
[46] J.F. Moulder, J. Chastain, Handbook of X-ray Photoelectron Spectroscopy: A Reference Book of Standard Spectra for Identification and Interpretation of XPS data, Physical Electronics, Eden Prairie Minnesota, 1995.
[47] N. Akhtar, G.R. Blake, R. Felici, H. Amenitsch, T.T.M. Palstra, P. Rudolf, Design of molecule-based magnetic conductors, Nano Res. 7 (2014) 1832–1842, https://doi.org/10.1007/s12274-014-0543-7.
[48] S. Kataoka, S. Banerjee, A. Kawai, Y. Kamimura, J.-C. Choi, T. Kodaira, K. Sato, A. Endo, Layered hybrid perovskites with micropores created by alkylammonium functional silsesquioxane interlayers, J. Am. Chem. Soc. 137 (2015) 4158–4163, https://doi.org/10.1021/jacs.5b00290.
[49] S. Rashid, C. Shen, X. Chen, S. Li, Y. Chen, Y. Wen, J. Liu, Enhanced catalytic ability of chitosan–Cu–Fe bimetal complex for the removal of dyes in aqueous solution, RSC Adv. 5 (2015) 90731–90741, https://doi.org/10.1039/C5RA14711E.
[50] D. Dasgupta, I.K. Shishmanova, A. Ruiz-Carretero, K. Lu, M. Verhoeven, H.P.C. van Kuringen, G. Portale, P. Leclère, C.W.M. Bastiaansen, D.J. Broer, A.P.H.J. Schenning, Patterned silver nanoparticles embedded in a nanoporous smectic liquid crystalline polymer network, J. Am. Chem. Soc. 135 (2013) 10922–10925, https://doi.org/10.1021/ja404825y.
[51] A. Longo, D.-J. Mulder, H.P.C. van Kuringen, D. Hermida-Merino, D. Banerjee, D. Dasgupta, I.K. Shishmanova, A.B. Spoelstra, D.J. Broer, A.P.H.J. Schenning, G. Portale, On the dimensional control of 2D hybrid nanomaterials, Chem. – A Eur. J. 23 (2017) 12534–12541, https://doi.org/10.1002/chem.201701493.
[52] S.A. Guda, A.A. Guda, M.A. Soldatov, K.A. Lomachenko, A.L. Bugaev, C. Lamberti, W. Gawelda, C. Bressler, G. Smolentsev, A.V. Soldatov, Y. Joly, Optimized finite difference method for the full-potential XANES simulations: application to molecular adsorption geometries in MOFs and metal-ligand intersystem crossing transients, J. Chem. Theory Comput. 11 (2015) 4512–4521, https://doi.org/10.1021/acs.jctc.5b00327.
[53] Z. Li, J. Kong, F. Wang, C. He, Polyhedral oligomeric silsesquioxanes (POSSs): an important building block for organic optoelectronic materials, J. Mater. Chem. C. 5 (2017) 5283–5298, https://doi.org/10.1039/C7TC01327B.
[54] K. Kato, M. Gon, K. Tanaka, Y. Chujo, Stretchable conductive hybrid films consisting of cubic silsesquioxane-capped polyurethane and Poly(3-hexylthiophene), Polymers (Basel) 11 (2019) 1195, https://doi.org/10.3390/polym11071195.